Available online at www.sciencedirect.com
ScienceDirect
Solid State Ionics 178 (2007) 249–252
SOLID STATE IONICS
www.elsevier.com/locate/ssi

Modeling of patterned mixed-conducting electrodes and the importance of sheet resistance at small feature sizes

Rupak Das, David Mebane, Erik Koep, Meilin Liu *

Center for Innovative Fuel Cell and Battery Technologies, School of Materials Science and Engineering, Georgia Institute of Technology, 771 Ferst Drive, Atlanta, GA 30332–0245, USA

Received 15 June 2005; received in revised form 2 April 2006; accepted 27 December 2006

Abstract

The sheet resistance of patterned electrodes was modeled and corrected using a finite volume technique. Results show that the sheet resistance of patterned electrodes may dramatically reduce the utilization or the performance of the electrodes when the feature size (e.g., thickness or width) is sufficiently small. Further, the utilization of a patterned electrode with a given geometry can be estimated, which may be used for correcting the sheet resistance effect on electrode performance. These results are important not only to fundamental study of electrode reaction mechanisms and kinetics but also to better design of porous mixed-conducting electrodes for solid oxide fuel cells.

Keywords: Mixed conductor; Patterned electrode; Simulations; Sheet resistance

1. Introduction

Computational approaches to analysis and optimization of fuel cell materials, components, and systems have attracted much attention in recent years [1–8]. While porous/dense mixed ionic-electronic conductors (MIECs) have been widely used as electrodes for SOFCs to reduce the interfacial polarization resistance [9–19], many fundamental issues still remain unanswered regarding geometrical aspects, electrode kinetics and transport mechanisms of dense electrodes. Increasingly popular analytical tools for uncovering answers to these questions are patterned electrodes and thin films of high aspect ratio. In many studies involving these cell structures, the electrical resistance (or sheet resistance) of the electrodes are recognized to exert a significant influence [3,9]. Brichzin et al. [3] made a correction to the interfacial resistance using a technique for calculating the effect of sheet resistance on utilization [11,14,16,18].

In this paper, the effect of sheet resistance on the utilization of patterned electrodes is quantitatively examined as a function of feature size. The geometrical parameters are varied in order to show the dependence of electrode polarization resistance and TPB utilization on the sheet resistance at different electrode thicknesses. While patterned LSM electrodes were used for this model study, our proposed computational approach is applicable to any patterned electrode. In our work we utilized the commercial CFD code Fluent.

2. Model formulation

We are not actually interested in modeling the sheet resistance itself, since sheet resistance is easily separated from interfacial resistance in the impedance spectrum. Rather, we are interested in modeling the effect that the sheet resistance has on the electrode polarization resistance through reduced activity along the MIEC at locations far from the current collector. As such, the focus of the model is on electrical transport within the MIEC, i.e., the movement of holes from the reaction sites to the current collector (or electrons from the current collector to the reaction sites).

The schematic configuration of the full-scale electrode system used for this calculation appears in Fig. 1. The current collector is placed as the topmost layer and has several stripes.

* Corresponding author. Tel.: +1 404 894 6114; fax: +1 404 894 9140.
E-mail address: meilin.liu@mse.gatech.edu (M. Liu).

0167-2738/$ - see front matter © 2007 Elsevier B.V. All rights reserved.
doi:10.1016/j.ssi.2006.12.021

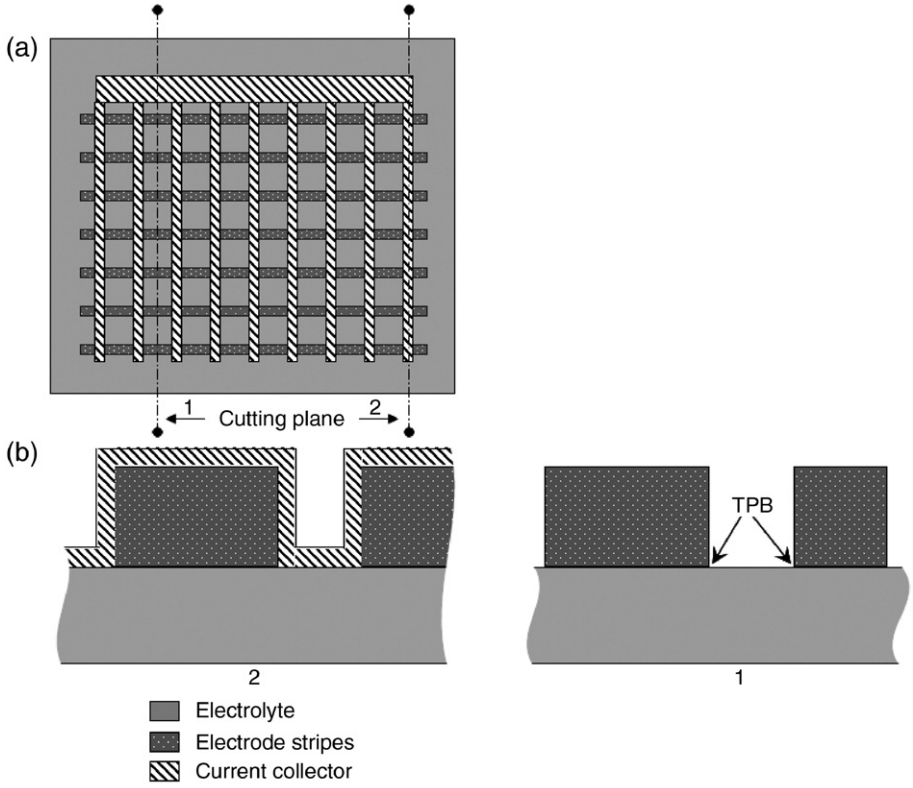

Fig. 1. (a) Top-view of the system, (b) cross-sectional view as seen through the cutting planes. The figure above is only a representation of the actual system which has 11 parallel current collector bars and 60 electrode stripes.

The stripes are connected at one end. The gap between each pair of successive stripes is 490 μm. The electrode bars are in 60 parallel rows below this layer. The bottom-most layer is the electrolyte (substrate).

The modeling was undertaken within the smallest symmetrical element – a single electrode bar – as schematically illustrated in Fig. 2. The solution was then extended to fit the whole system geometry depicted in Fig. 1. The specifications for the modeled electrode bar are $245 \times 25 \times (0.06–3.2)$ μm. The figure shows the manner in which the current collectors and cathode strips are placed in an orthogonal grid on the substrate. The (platinum) current collector has a much higher electrical conductivity than that of the electrodes (LSM) and is presumed to maintain a uniform potential throughout.

Laplace's equation $\nabla^2\phi = 0$ is solved as the constitutive equation in the bulk of the MIEC domain, where ϕ is the electrostatic potential of the system. Platinum current collectors are given a fixed value via the Dirichlet condition. To calculate the primary current distribution, the entire triple phase boundary (TPB) length, modeled as a rectangular strip of ~ 1 nm height along the length of the TPB, is assumed to be equipotential at 0 V (Dirichlet condition). The insulated boundary conditions are designated with the Neumann boundary condition and the normal flux or the gradient of the electrostatic potential at those surfaces is zero. The electrical conductivity of LSM is taken to be 38 S/cm at 750 °C [3]. In order not to short-circuit the system, a very thin sheet of 0.5 μm width of the same material as the electrode is put in between the TPB ends and the current collectors. The thickness of the electrode was varied, keeping the other geometrical parameters constant throughout the study. The thicknesses of the cathode studied were 0.06, 0.12, 0.18, 0.6, 0.77, 2.5 and 3.2 μm.

To calculate the secondary current distribution, the effective resistance of the smallest symmetrical cathode element has been calculated from the experimental data (using pattern heights

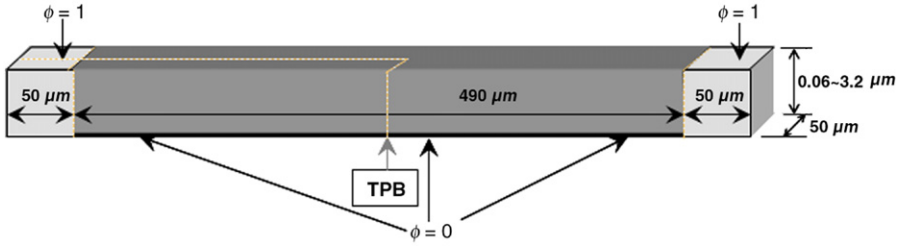

Fig. 2. Perspective view of the single cathode bar.

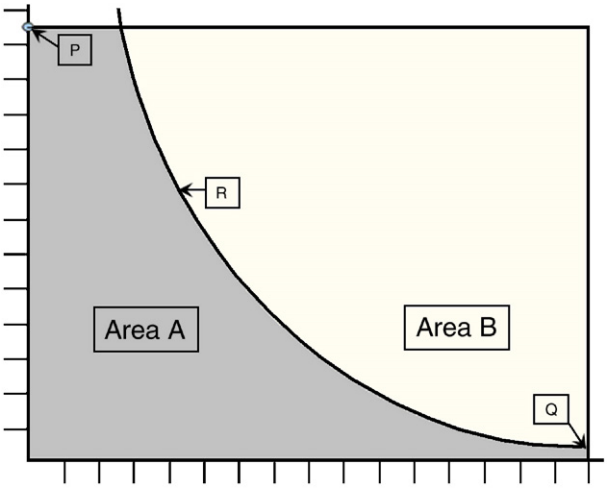

Fig. 3. Percent utilization: Area A is the integrated area under the current density curve capped by the baseline current density value, summation of Area A and Area B is the total Area that corresponds to the uniform baseline value current density, point *P*, *Q* and *R* are respectively the baseline current density from 3.2 μm case, current density value at the middle of TPB of any case and the current density distribution curve.

where full TPB utilization is assumed) and input at the TPB as the contact resistance. This is accomplished by creating a second domain of very high conductivity whose interface with the MIEC is along the TPB.

The correction for sheet resistance was accomplished through two methods. At first, the sheet resistance was calculated directly from the model. Second, a correction to the active area of the cathode strip can be made by comparing simulations between geometries where we assume 100% utilization and those where we assume an influence of sheet resistance. With reference to the series of data taken at 750 °C in Ref. [9], the baseline current density for 100% utilization was calculated by assuming that the cathode geometry of 3.2 μm thickness was 100% utilized, taking the current density at the TPB at the halfway point between current collectors. As shown in Fig. 3, the ratio of the integrated area under the current density curves (Area A) along the TPB

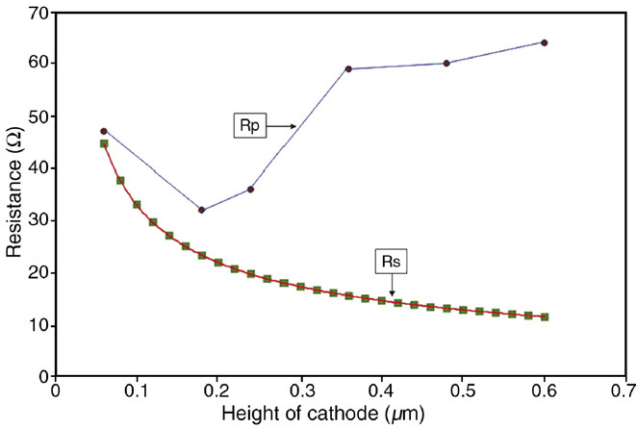

Fig. 4. Comparative plot of sheet (R_s) and interfacial resistances (R_p) against electrode thickness.

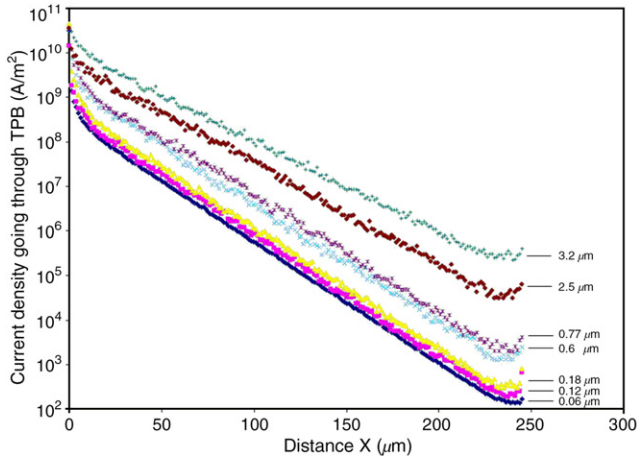

Fig. 5. Comparison of current density distributions along the TPB against the distance (X) from the left edge of the TPB. The numbers adjacent to each curve represents the thickness of respective cathodes.

capped by the baseline current density (Area B + Area A) yields percentage utilization for the TPB. Because of the high aspect ratio of the cathode bar, this correction for utilization should hold (given the correct baseline current density) even if the electrical current passes through the surface outside of the defined TPB width.

3. Results and discussion

Fig. 4 portrays the relationship between heights of the cathodes in microns and the resistance (interfacial, from experiment, and sheet, calculated) in ohms. The upper limit of cathode height depicted here is 0.6 μm. Fig. 5 shows the current density distributions along the TPB (against the distance from the left edge of the TPB in semi-log scale) for different heights of the single cathode bar, which spans from 0.06 μm to 3.2 μm.

It seems that the sheet resistance values have followed a nearly linear relationship starting from 0.6 μm to 0.3 μm

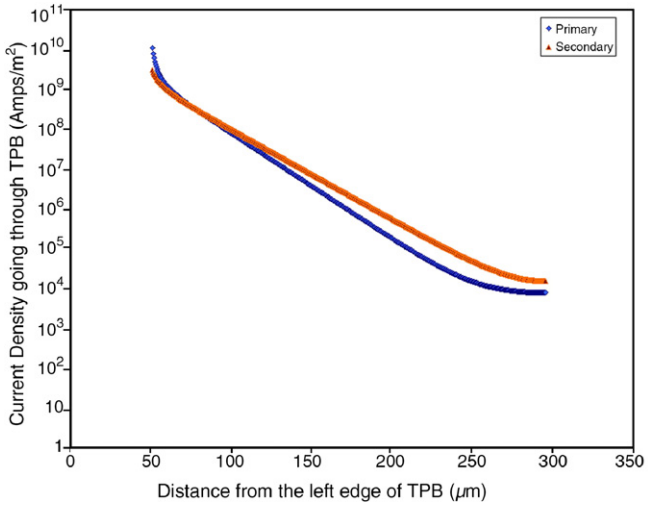

Fig. 6. Comparison of the primary and secondary current densities for 0.06 μm cathode thickness.

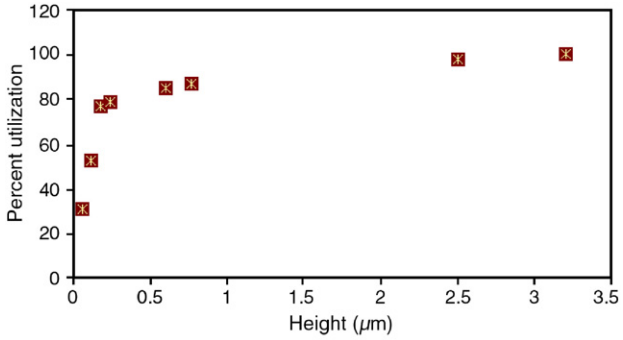

Fig. 7. Percent utilization of the electrodes.

cathode height. Below that cathode height, the sheet resistance began to increase rapidly. Experimentally the minimum in the interfacial resistance is noted near 0.18 μm. Fig. 5 also shows that the values of the current density distributions broaden when the thickness of the electrodes increase.

A comparative study between primary and secondary current calculations is shown in Fig. 6 on the 0.06 μm cathode thickness case. The difference between the curves is not particularly large; nevertheless, the secondary current distribution is used in the correction for percent utilization expressed in Fig. 7. Clearly, the thinner the electrode the lower the percent utilization; however, the utilization reaches a high asymptotic value beyond 2.5 μm thickness. The asymptotic trend validates the decision to use the 3.2 μm-thick cathode as the baseline case [9].

The trend in Fig. 7 shows that the percent utilization of the cathode increases with the height of the cathode as the sheet resistance of the electrode is reduced. The slope of the curve in the figure changes at the cathode thickness of 0.18 μm. The percent utilization seems to increase with a much greater slope until this thickness and then changed to less steep slope thereafter. This corresponds to the maximum in conductance with height seen in the experimental data. The correction to the overpotential is made by multiplying the conductance (or reciprocal resistance) by Area A/total area, in reference to Fig. 3. The corrected conductance data appears in Ref. [9].

4. Conclusions

Sheet resistance in high aspect ratio patterned cathodes has been analyzed, and a method of correcting the interfacial resistance in these cathodes based on the utilization of the electrode has been devised. The analysis tends to reinforce the view that the sheet resistance phenomenon is the cause of the maximum in interfacial conductance with respect to pattern height seen in the impedance data for these patterned cathodes. The overpotential due to sheet resistance likely exceeds that due to electrode polarization resistance at the smallest pattern heights and at points furthest from the current collector. Sheet resistance can indirectly affect the measured electrode polarization resistance by limiting the utilization of the cathode. The framing of the problem in terms of utilization stems from the fact that most impedance spectra are analyzed under the assumption that the cathode-electrolyte interfaces are equipotential in a given experiment. Experimental data casts doubt on this, but our method provides a relatively simple correction under which this assumption can be restored.

Acknowledgments

This work was supported by DOE-NETL SECA Core Technology Program under Grant No. DE-FC26–02NT41572.

References

[1] Mogens Mogensen, Steen Skaarup, Solid State Ionics 86–88 (1996) 1151.
[2] Hiroshi Fukunaga, Manabu Ihara, Keiji Sakaki, Koichi Yamada, Solid State Ionics 86–88 (July 1996) 1179 (Part 2).
[3] V. Brichzin, J. Fleig, H.U. Habermeier, G. Cristiani, J. Maier, Solid State Ionics 152–153 (December 2002) 499.
[4] Fuel Cells – A Handbook, revision 6, U.S. Department of Energy.
[5] Femlab User's Manual version 3.0, Comsol Inc.
[6] S. Skinner, International Journal of Inorganic Materials 3 (2001) 113.
[7] M. Liu, Journal of the Electrochemical Society 145 (1998) 142.
[8] J. Fleig, Journal of Power Sources 105 (2002) 228.
[9] Erik Koep, Charles Compson, Rupak Das, David Mebane, Meilin Liu, Electrochemical and Solid-State Letters 8 (2005) A592.
[10] J. Fleig, Annual Review of Materials Research 33 (2003) 361.
[11] A.J. McEvoy, Solid State Ionics 132 (2000) 159.
[12] E. Koep, C. Compson, M. Liu, Solid State Ionics 176 (2005) 1.
[13] B.C.H. Steele, Solid State Ionics 86 (1996) 1223.
[14] O. Yamamoto, Y. Takeda, R. Kanno, M. Noda, Solid State Ionics 22 (1987) 241.
[15] M. Liu, Z. Wu, Solid State Ionics 107 (1998) 105.
[16] J. Mizusaki, H. Tagawa, K. Tsuneyoshi, A. Sawata, Journal of the Electrochemical Society 138 (1991) 1867.
[17] R. Radhakrishnan, A. Virkar, S. Singhal, Journal of the Electrochemical Society 152 (2005) A210.
[18] M. Suzuki, H. Sasaki, S. Otoshi, A. Kajimura, N. Sugiura, M. Ippommatsu, Journal of the Electrochemical Society 141 (1994) 1928.
[19] V. Brichzin, J. Fleig, H.U. Habermeier, J. Maier, Electrochemical and Solid State Letters 3 (2000) 403.